Materials Advances

ROYAL SOCIETY OF CHEMISTRY

PAPER

View Article Online
View Journal | View Issue

Cite this: *Mater. Adv.*, 2026, 7, 1099

Mechanically driven bacteria-based crack detection

Ellen W. van Wijngaarden,[ab] Tyrone Chen,[c] Ilana L. Brito,[bd] Nikolaos Bouklas,[abe] Andrea Giometto[bf] and Meredith N. Silberstein*[ab]

Received 13th September 2025,
Accepted 1st December 2025

DOI: 10.1039/d5ma01053e

rsc.li/materials-advances

Early detection of fatigue cracking is critical for extending the lifetime of structural materials and reducing waste from premature part replacement or over-engineering. Current detection methods, such as strain sensors and ultrasonic testing, are costly, maintenance-intensive, and lack any built-in response to damage. Here, we present a durable engineered living coating that enables *in situ* crack detection of conventional structural materials. The coating integrates bacterial spores within a tailored synthetic polymer matrix, combining the mechanochemical control of the matrix with the biological responsiveness of the spores. Upon crack formation, the coating produces a fluorescence signal that directly reports damage under diverse loading conditions, geometries, and material systems. This biohybrid platform establishes a scalable and generalizable strategy for sustainable material design. Beyond detection, the modular spore-polymer architecture offers potential for next-generation multifunctional coatings capable of not only sensing but also mitigating crack propagation. This work demonstrates a new approach for integrating living components onto structural materials to enhance their durability, safety, and sustainability.

All materials eventually fail. Repeated loading and everyday use of materials and structures leads to fatigue cracking and ultimately, failure over time.[1–6] Engineers are continuously working to design fatigue resistant materials with higher toughness and improved elasticity. Considerable progress has been made in designing tougher materials with various mitigation strategies to prevent fatigue cracking.[5,7–9] Nonetheless, early crack detection remains essential for safety to prevent catastrophic failure in infrastructure and equipment such as bridges, oil and gas vessels, aircraft fuselages, piping, power plant equipment, and boat hulls.[10] Early detection of fatigue cracks is important for safety as well as for minimizing material waste through increased product lifespan and reduced over-engineering.

Current materials lack the ability to sense and respond to cracks, calling for innovative design solutions for stimuli-responsive materials. Nature provides many examples of materials with advanced functionalities, including responses to environmental stimuli and self-healing, that surpass existing synthetic material capabilities. Biomaterials, such as bone and plant tissue, demonstrate the ability to sense damage and then allocate resources to facilitate a response, for example in the form of hormone signaling or healing.[11,12] Bio-inspired strategies, such as vascularization, embedded capsules, and intrinsic dynamic bonds aim to mimic biological sense-and-response to enable healing of a damaged region. However, these strategies each have their own limitations, for example compatibility with only a narrow set of chemistries or only working for a single damage event.[13–20] Researchers have addressed some of these limitations by incorporating biological organisms. Previous work in this field has produced many examples of futuristic living materials capable of sensing, adapting, and responding to diverse signals and stimuli.[14,21–27] Unfortunately, the challenge of integrating and maintaining living components often prevents the use of biological approaches to expand material functionality.[28–31] This roadblock has prevented researchers from harnessing living materials to extend material lifespan, calling for innovative biological and material design solutions. A possible strategy is to design materials with biological sensing components and structural synthetic components. These hybrid living coatings may be the ideal solution for the ubiquitous problem of fatigue cracking in conventional materials, providing early crack detection and the potential for future autonomous crack mitigation, surpassing existing crack detection strategies.

Current crack detection methods often require regular inspection or can be destructive. Methods, such as visual inspection and dye penetrant testing, are labor intensive or

[a] *Sibley School of Mechanical and Aerospace Engineering, Cornell University, Ithaca, New York, USA, meredith.silberstein@cornell.edu*
[b] *Engineered Living Materials Institute, Cornell University, Ithaca, New York, USA*
[c] *Materials Science and Engineering, Cornell University, Ithaca, New York, USA*
[d] *Meinig School of Biomedical Engineering, Cornell University, Ithaca, New York, USA*
[e] *Pasteur Labs, Brooklyn, New York, USA*
[f] *School of Civil and Environmental Engineering, Cornell University, Ithaca, New York, USA*

decrease the structural performance of the component.[32–35] Electrical or optical strain sensors can be embedded in some materials, or alternatively, attached to the surface and are non-destructive alternatives, but still require contact.[36–39] Non-contact methods, including applying acoustic, ultrasonic, and eddy currents, are typically used for monitoring over the long-term and for large regions. However, these methods are sensitive to noise and debris, which limits detection to primarily actively growing cracks.[10,36,40–46] Additional studies of deformation and damage- and plasticity-detection in structural polymers have made use of mechanochromic activation to obtain fluorescence or a color change in the region of material deformation.[16,47–50] Current crack detection methods and equipment can be costly, may require equipment downtime, may not be optimal for detection of sub-millimeter cracks covered with dirt, debris, or paint, and largely do not provide pathways for mitigation.

We introduce a spore-polymer material coating to provide a generalized strategy for structural material crack detection and response. The use of spores that are innately resistant to UV exposure, lack of nutrients, temperature and pH shifts, and mechanical abrasion, will allow our coating to maintain functionality after polymer curing and during component use.[51–54] Active cells that germinate from the spores offer diverse biochemical functionality to the coating. The synthetic polymer provides control of the chemical environment, and transduces impending damage in the substrate into a coating response. When the structural material undergoes local plastic deformation in the process of cracking, our composite coating cracks to expose the spores to nutrients and germinants, which induces spore germination and allows vegetative cell growth. The active cells fluoresce or produce other signals, such as luminescence or pH changes, to enable crack detection. Our coating can detect and respond to fatigue cracks, addressing the need for non-destructive, continuous crack monitoring of structural materials. A bacteria cellular response to deformation of the structural material can thus assist in early detection of damage. The hybrid coating also offers future potential for genetic engineering to realize crack mitigation strategies. We demonstrate that our coating can successfully detect and respond to cracks *in situ* by detecting regions of plasticity ahead of a propagating crack, support living cells without an external nutrient source, and can be applied to different structural materials in various loading environments. Real world use of this coating will improve safety and reduce material waste through increased product lifespan.

1 Results and discussion

1.1 Material selection and design of living coating for crack detection

Bacterial spores are a natural choice as a living component of a coating for fatigue crack detection. Spores do not require nutrients in the spore state and are also resistant to many external perturbations, ideal characteristics for fatigue detection, which requires long periods of inactivity (weeks to years) followed by short periods of activity (hours to days). However, spore engineering is in its infancy, with relatively few cues that spores will germinate in response to.[55–60] Furthermore, the spores must be spatially distributed on the structural material of interest. Therefore, we cannot simply "use spores to detect cracks", but rather the spores must be integrated into a material system to produce a functional coating. We take inspiration from the self-healing concrete literature, and use hydration and distribution of germinants as the trigger for spore germination.[14,61–65] We connect this to the desired input trigger (fatigue cracking of an arbitrary structure) by integrating the spores into a water impermeable polymer that develops microcracks at a low strain threshold. These microcracks in the coating remain open for water, nutrients, and germinants to permeate with any local accumulation of plastic strain in the structural substrate – a signature of a propagating process zone in the near-crack tip region. In contrast to spore engineering, engineering of bacterial cell behavior in the vegetative state is advanced, particularly for model organisms. There are therefore a range of options to make the vegetative cells outgrown from spores visible – fluorescence is demonstrated here. This concept for detecting the onset of fatigue fracture is shown schematically in Fig. 1.

The spore component of the functional coating is required to have fast germination and proliferation for quick detection. Working with a genetically tractable organism enables genetic modifications to aid detection (*e.g.*, *via* fluorescence or bioluminescence) and to implement mitigation responses to enable

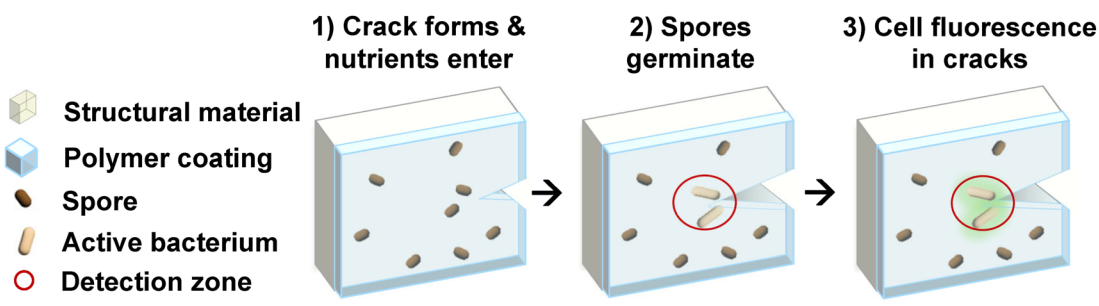

Fig. 1 Schematic of crack detection mechanism for a structural material based on a spore-polymer coating. When the structural material undergoes plastic deformation or initiation of a ductile fracture process, the coating cracks, allowing nutrients to enter and leading to spore germination. The spores then germinate into vegetative cells that fluoresce, enabling crack detection *via* fluorescence imaging.

modification for visualization *via* fluorescence, bioluminescence, or other signals to enable responsive behavior. *Bacillus subtilis* spores were selected based on their common use in previous literature,[66,67] demonstrated fast growth of vegetative cells, with a doubling time of approximately 30 minutes in ideal conditions, and the availability of a large synthetic biology toolkit. Here, we used a strain of *B. subtilis* that was modified to constitutively express green fluorescent protein (GFP) in the vegetative cell state. We compared the germination and subsequent growth dynamics, as measured by optical density, of our spores to those of a commercially available *B. subtilis* to demonstrate that the fast growth was unchanged and that the fluorescent signal was strong enough for detection (Fig. S1, SI).

The polymer matrix for the hybrid living coating was selected based on five main requirements: non-cytotoxicity to *B. subtilis*, embedded spore revivability, brittle mechanical behavior, water/nutrient broth impermeability, and transparency. Accordingly, four material candidates were initially selected for evaluation. An epoxy was selected due to prominent use of epoxies in literature that indicated biocompatibility and convenient fabrication methods.[68] Three other materials used in biocompatible coatings were also selected for additional testing: tetEGDA,[69] PEMA,[70] and PMMA.[71,72] Literature also indicated thermal stability and stiffness similar to common non-gel cell culture substrate materials ($E \approx 1$ GPa) for these candidates.[70,73,74] The four transparent selected materials were investigated further based on the requirements for non-cytotoxicity, brittleness, and revivability only upon matrix cracking.

Biocompatibility of the matrix material candidates was first tested to ensure that the *B. subtilis* cells could grow when in contact with the polymer matrix. Cytotoxicity results indicate that PEMA and PMMA are the most biocompatible due to no growth inhibition around samples of these materials, as seen in Fig. 2a. All trials for the cytotoxicity tests are shown in Fig. S2a (SI). Uncured methylmethacrylate was also later tested to ensure that the unpolymerized monomers of PMMA were also non-cytotoxic (Fig. S2b, SI).

Uniaxial tensile tests were conducted to evaluate the strain to failure of the different material candidates before spores were embedded (Fig. 2b). The coating requires a brittle behavior at small strains to successfully detect plastic deformations of the structural substrate. Uniaxial tensile tests indicated low strain to failure (<10% elongation) for all materials except for PEMA. All candidates had a Young's modulus ≈ 1 GPa except for tetEGDA, however the stiffness of tetEGDA (0.22 GPa) is still above that of bacterial cells (0.15 GPa).[75–77] A graph of the low strain values is included for close up visualization in Fig. S2c (SI). All tensile testing trials for each material candidate is included in Fig. S3a–d (SI) and results for Young's modulus, ultimate tensile stress, and strain to failure are summarized in Table S1 (SI). PMMA showed the smallest strain to failure at 1.08%, demonstrating small strain brittle behavior that is ideal for the coating matrix material.

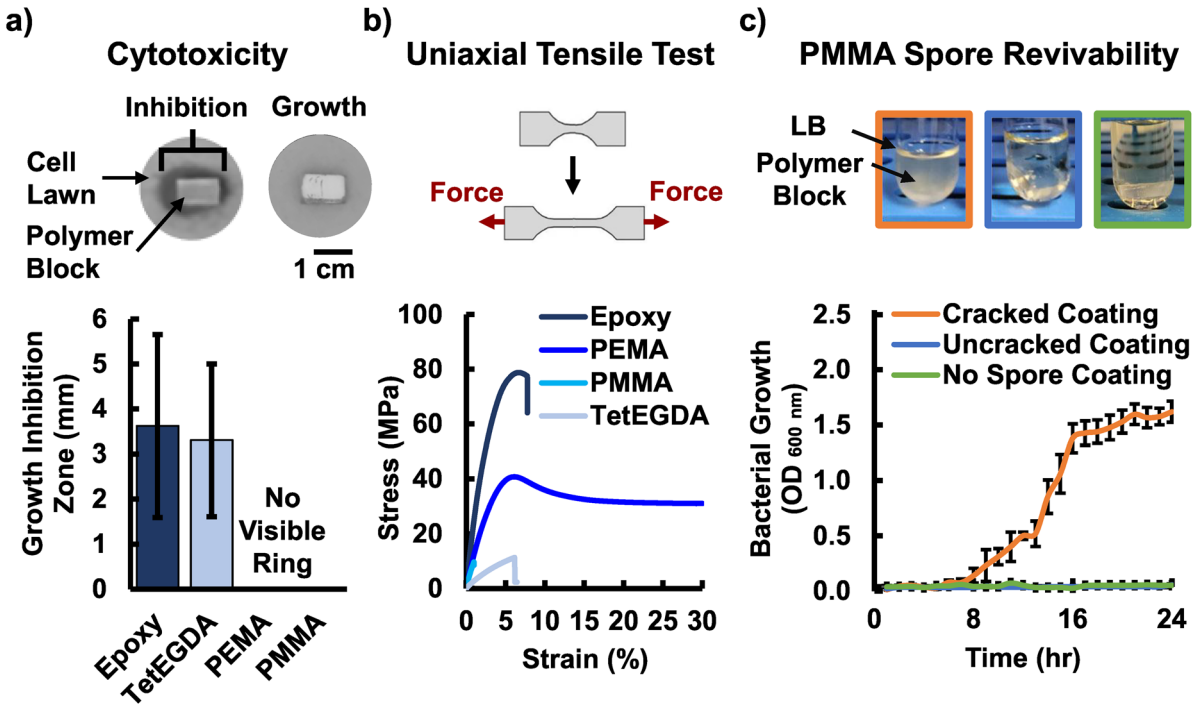

Fig. 2 The matrix material for the spore-polymer composite coating was selected based on (a) material non-cytotoxicity shown *via* the lack of a growth inhibition zone (quantified by [the polymer block width subtracted from the diameter of inhibition zone] divided by 2), (b) mechanical properties including strain to failure and Young's modulus, and (c) embedded spore revivability (PMMA test shown here) where growth was measured for cracked spore-polymer coating (green), uncracked spore-polymer coating (orange), and coating without spores (blue) samples. PMMA was selected as the ideal polymer matrix due to biocompatibility, brittle mechanical behavior, and spore revivability. All error bars report standard error of the mean (n = 3).

Table 1 Summary of material selection process for the polymer matrix based on requirements of mechanical properties and biocompatibility. PMMA was selected as the best candidate

Material	Cytotoxic	Brittle	Revivable spores
Epoxy 4500	Yes	Yes	—
tetEGDA	Yes	No	—
PEMA	No	No	—
PMMA	No	Yes	Yes

The remaining material candidate, PMMA, that met the requirements for non-cytotoxicity and brittle mechanical behavior was tested both for spore revivability upon matrix cracking and absence of germination in the absence of matrix cracking (Fig. 2c). Note that there was no background spore growth without cracks, as a second, spore free coating of PMMA fully encapsulated spores for complete biocontainment. A primary concern was that polymer cure strains or uncured monomers may affect bacterial revivability once embedded in the coating.[78] Spores, methylmethacrylate monomer, and initiator were mixed at a 1% w/v ratio of spores to monomer and cured as a coating on polycarbonate blocks (as a representative substrate). A layer of methylmethacrylate monomer and initiator without spores was then applied on the top surface and cured to ensure that no spores were exposed at the surface of the coating. This hybrid living coating was manually cracked under a bending load and then placed in Lysogeny broth (LB) growth media for 24 hours. The number of cycles to induce fatigue cracking can range from a few to ten million cycles which might occur over the span of years. Often fatigue cracking occurs over the span of years with factors such as temperature and loading waveform playing a key role.[79] Cell germination and growth was apparent from the increasingly cloudy appearance of the medium over time, which was quantified through optical density measurements (Fig. 2c). In the absence of surface cracking, the medium remained clear, indicating that the intact PMMA matrix was negligibly permeable to nutrients and embedded spores did not germinate. As expected, blocks coated in neat PMMA (no spores) did not show signs of vegetative cell growth. Collectively, these results show that PMMA is a non-cytotoxic matrix material for embedding spores and does not prohibit spore germination and cell growth upon nutrient exposure due to matrix cracking. The material selection process leading to the selection of PMMA as the polymer matrix is summarized in Table 1.

1.2 Detection of structural material deformation using a hybrid living spore-polymer coating

To determine the coating's ability to detect the structural deformation through the sequence of coating cracking, spore germination, and subsequent cell fluorescence, dog bone samples of polycarbonate (a ductile and transparent glassy polymer) coated with the spore-PMMA composite were subjected to tensile testing (Fig. 3a). Samples were then given 24 hours of growth time in a nutrient bath with no applied tensile force. Under these conditions, cracks are not expected to grow further. Samples were then imaged using fluorescence microscopy. Note that coating the glassy polymer (polycarbonate) did not have a statistically significant effect on the Young's

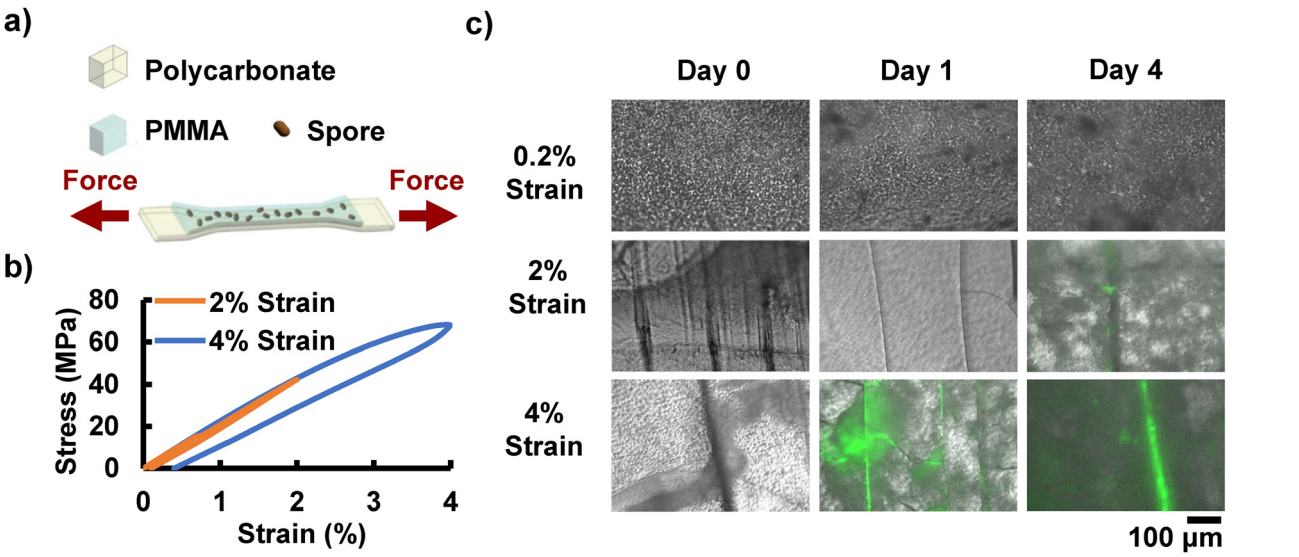

Fig. 3 Mechanically driven crack detection demonstrated *via* cracks in the spore-PMMA coating detected when the underlying substrate underwent plastic deformation. (a) Schematic of polycarbonate dog bone sample coated with the spore-polymer composite coating for crack detection and subjected to uniaxial tensile testing. (b) Cyclic stress–strain curves for coated polycarbonate samples tested at 2% and 4% strain demonstrating the elastic and plastic behavior for the strain levels respectively as indicated by the amount of residual strain. (c) No fluorescence was observed for samples at Day 0 just after testing as cells had not yet grown. Samples tested until 0.2% strain did not crack and did not show any fluorescent signal. Crack fluorescence was first detected at Day 1 for samples subjected to 4% strain. Fluorescent signal was much stronger at Day 4 with high background fluorescence due to culture growth in the surrounding medium. Samples tested until 2% strain showed negligible crack fluorescence at Day 1 and limited crack fluorescence at Day 4.

modulus, using a two-tailed student *t*-test (Fig. S4, SI). Samples were tested to different levels of deformation, including 0%, 0.2%, 2%, and 4% strain (Fig. 3b and Fig. S5a–c, SI). Note that plastic yielding for polycarbonate occurs at approximately 2% strain in uniaxial tension, as indicated by the inelastic strains observed upon unloading (Fig. 3b and Fig. S5d, SI). As expected, deforming the coated specimens to 2% and 4% strain resulted in cracking of the coating, whereas cracking did not occur for lower strains. Consequently, no fluorescence was observed in the samples subjected to 0% or 0.2% strain (Fig. 3c and Fig. S6, SI). Specimens tested to 4% strain showed fluorescent cracks in the matrix at 24 hours of growth in LB media (Fig. 3c and Fig. S6, SI), indicating that the cracks enabled the nutrient bath to penetrate the coating, leading to spore germination and then cell growth. Interestingly, samples with 2% strain displayed a predominantly elastic response and consequently later onset of fluorescence (apparent at 4 days). The faster fluorescence response for the 4% strain samples compared to 2% strain samples is likely due to the plastic deformation of the polycarbonate substrate holding the cracks in the PMMA open and allowing nutrients and water to flow into the cracks more easily (Fig. S6 and S7, SI). This presents a way to practically distinguish between cracks that may be the result of external action through handling the coating, compared to deformation or cracking within the structural material itself. Fig. S7 (SI) provides a zoomed in image in which cells can be identified in the wispy pattern along the fluorescent cracks. By day four, the 4% strain samples show significant overgrowth from the original crack pattern. No fluorescence is observed at any mechanical strain when no spores are embedded in the PMMA (Fig. S6).

1.3 *In situ* detection of localized deformation

The spore-PMMA coating was further enhanced to function independently (no external nutrient bath required), and then used to demonstrate *in situ* monitoring and detection of the structural material deformation, including complex geometries with regions of concentrated stress. A gel layer was added on top of the spore-PMMA layer to supply nutrients to spores and cells *via* cracks. The nutrient layer would enable the coating to be used in ambient dry environments for practical applications. The gel was required to be biocompatible in order to not inhibit cell viability or proliferation. The layer was also designed to have a high strain to failure to maintain cohesion and contact when cracks appear in the underlying spore-PMMA layer. Various gels traditionally used as bacterial substrates were considered for this layer based on the biocompatibility and stretch requirements (Fig. S8, SI). We tested biocompatibility of gel candidates by growing bacteria on gel plates to determine if the gels enabled cell growth (Fig. S8a, SI). Mechanical properties were measured through uniaxial tensile testing of gel dog bone samples for each candidate material. Based on test results, polyacrylamide (pAAM) was chosen due to fast and extensive bacterial growth indicating biocompatibility, and high stretch to failure (Fig. S8b, SI). The gel layer recipe, specifically the fraction of crosslinker and initiator, were tuned to improve diffusivity of nutrients (Fig. S9a–e). A compliant, water impermeable layer was added on top of the nutrient layer to keep the gel layer hydrated. It is essential that the gel layer stays hydrated, so that it can deliver nutrients to the spores *via* the cracks when they are triggered by structural material deformation.[77] UV-cured silicone was selected as the water proofing layer for its ability to best keep the gel hydrated and adhere the gel to the structural material (Fig. S10a, SI). The silicone layer had sufficiently high strain to failure to ensure that it would not fail before the structural material (Fig. S10b). Ideal detection conditions would be indoors to avoid environmental weathering with temperatures above freezing to avoid damage to the gel layer. A sufficient silicone seal prevented drying out at typical room temperatures and humidity levels of approximately 20 °C and 30% humidity for several days. Samples remained hydrated for over 28 days when in humidity conditions of 95%. The time scales for polymer aging are estimated to be approximately 25 years for PMMA and 20 years for silicone materials at 20 °C.[80–82] However, drying of the nutrient layer occurs over a much shorter period. While the PMMA layer is adhered to the structural materials in this study, the gel layer is not adhered to the underlying PMMA layer, which may facilitate replacing the nutrient layer if needed. Alternative gel layers or gel surface treatments could be used if adhesion were required for a particular application, provided that the gel still meets the design criteria outlined: biocompatibility and high strain to failure.

The complete coating, consisting of the spore-PMMA layer, nutrient layer, and silicone layer, was tested to ensure that there was no spontaneous germination and that the complete coating could successfully detect cracks. Polycarbonate dog bone samples with the complete coating were stored for 4 weeks in a humidity chamber and checked each week to monitor if there was spontaneous germination. No spontaneous germination was observed after 4 weeks (Fig. S11, SI), indicating the need for cracks for the nutrients to reach the embedded spores. This also demonstrates potential storage for the material before application to a structural material or possible humidity conditions for longer term coating use. To test crack detection with the complete coating, dog bone samples were tested under uniaxial tension to 0%, 2%, and 4% strain as per the previous tests conducted in the nutrient media bath to demonstrate similar crack detection trends (Fig. S12, SI). Faint cracks could be detected in the 4% strain sample at 24 hours, with significant overgrowth seen by day 4. Samples tested to 2% strain showed limited fluorescence at 24 hrs and stronger response by day 4, whereas samples subjected to 0% strain showed no response. Specimens that had been stored for 4 weeks were also tested at 4% strain and demonstrated successful crack detection (Fig. S11b and c, SI) post storage.

Next, a new specimen geometry was selected to demonstrate the coating's effectiveness for detecting localized damage. A stress concentration in the form of a circular cutout in the polycarbonate structural layer was added to a widened dog bone geometry (Fig. S13a, SI). The samples were subjected to monotonic loading to a crosshead displacement of 4% of the initial grip-to-grip distance, exhibiting first linear elasticity and

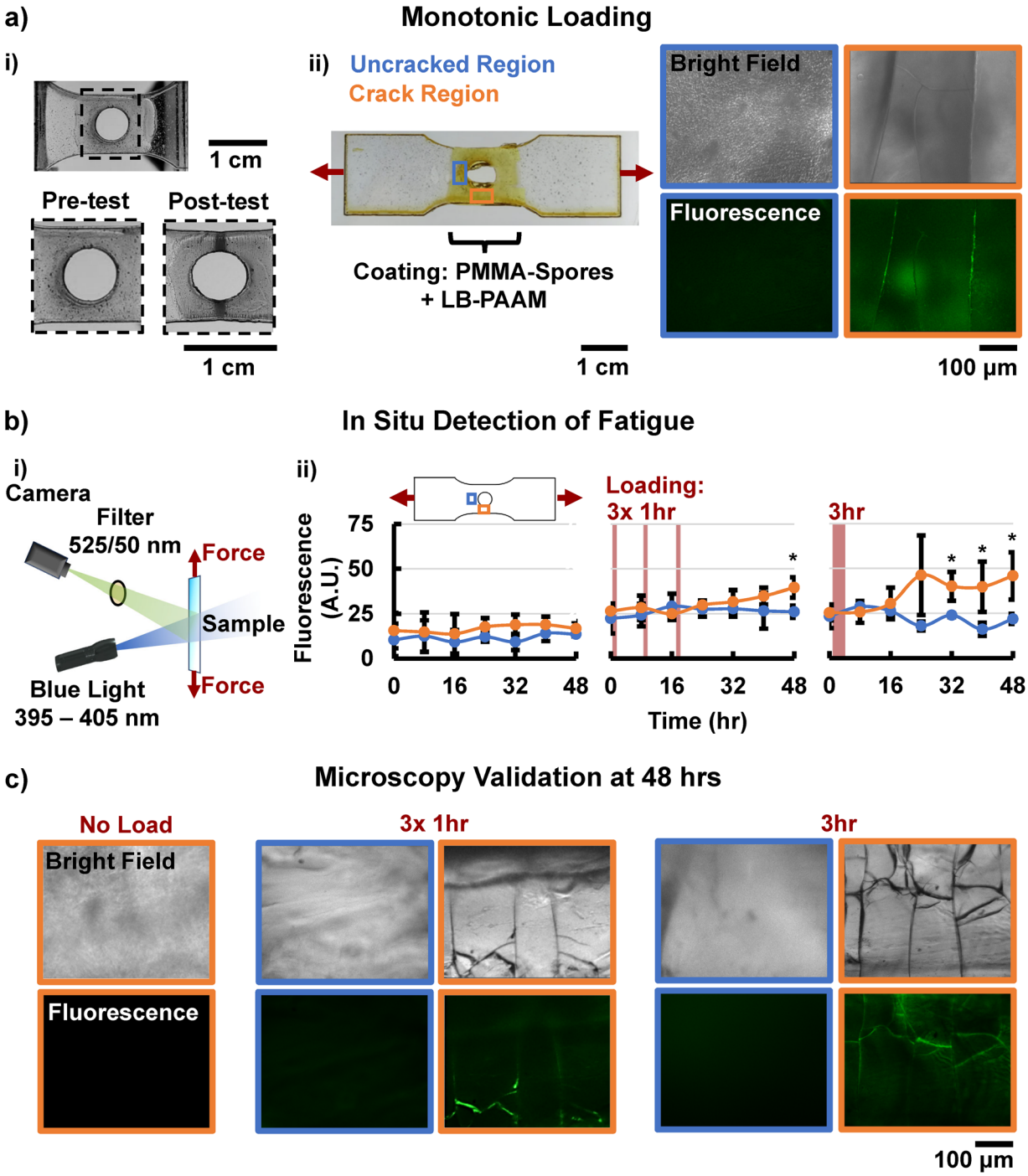

Fig. 4 *In situ* detection of localized cracks. (a) (i) Image of sample coated region pre-testing and post-testing showing cracks concentrated in the high-stress regions of the sample. (ii) Microscopy results for a sample loaded monotonically to 4% strain with a nutrient layer added showing no cracks and fluorescent response in the no-stress region and crack detection in the region of localized stress. (b) (i) Schematic of *in situ* fluorescence imaging setup consisting of a blue light for excitation, sample being tensile tested, filter and camera for capturing GFP fluorescence. (ii) Fluorescence responses for the low stress region beside the hole with no cracks and the high stress region above/below the hole with cracks were measured over a time period of 48 hours. Samples with no loading did not show any cracks or fluorescence when imaged using microscopy at 48 hours. Samples that underwent 1 hour of loading showed surface level cracks but no significant fluorescence response (Fig. S17, SI). Samples that were intermittently loaded for a total of three hours showed a statistically significant fluorescence response at 48 hours and clear fluorescent crack regions. Samples that underwent 3 hours of loading immediately had the most growth time and showed the strongest fluorescence response which was statistically significant by 32 hours as measured with the *in situ* imaging setup. Cyclic tensile testing was performed at 100 N, 0.03 Hz. All error bars report standard error of the mean (n = 3). (c) Microscopy images validating the *in situ* fluorescence imaging setup taken at the 48 hour time point in the region of stress concentration.

then yielding (Fig. S13b, SI). The stress concentration resulted in localized cracking in the coating at the top and bottom of the circular cutout (Fig. 4a(i)). Digital image correlation results on neat polycarbonate specimens indicate that, as expected, maximum principal strain at the top and bottom of the circle (Fig. 4a(i)) surpasses 4% (Fig. S14, SI), and therefore that plastic deformation will occur at the top and bottom as shown in Fig. 4a(i). Microscopy conducted on the coated specimen 24 hours post-test indicated successful crack detection as expected in the cracked regions and no cracks or fluorescence in the meridional edge of the hole, which experienced low stress and strain levels (Fig. 4a(ii) and Fig. S15, SI).

The majority of cracks in a structural layer form over an extended period of time due to small cyclic loads or

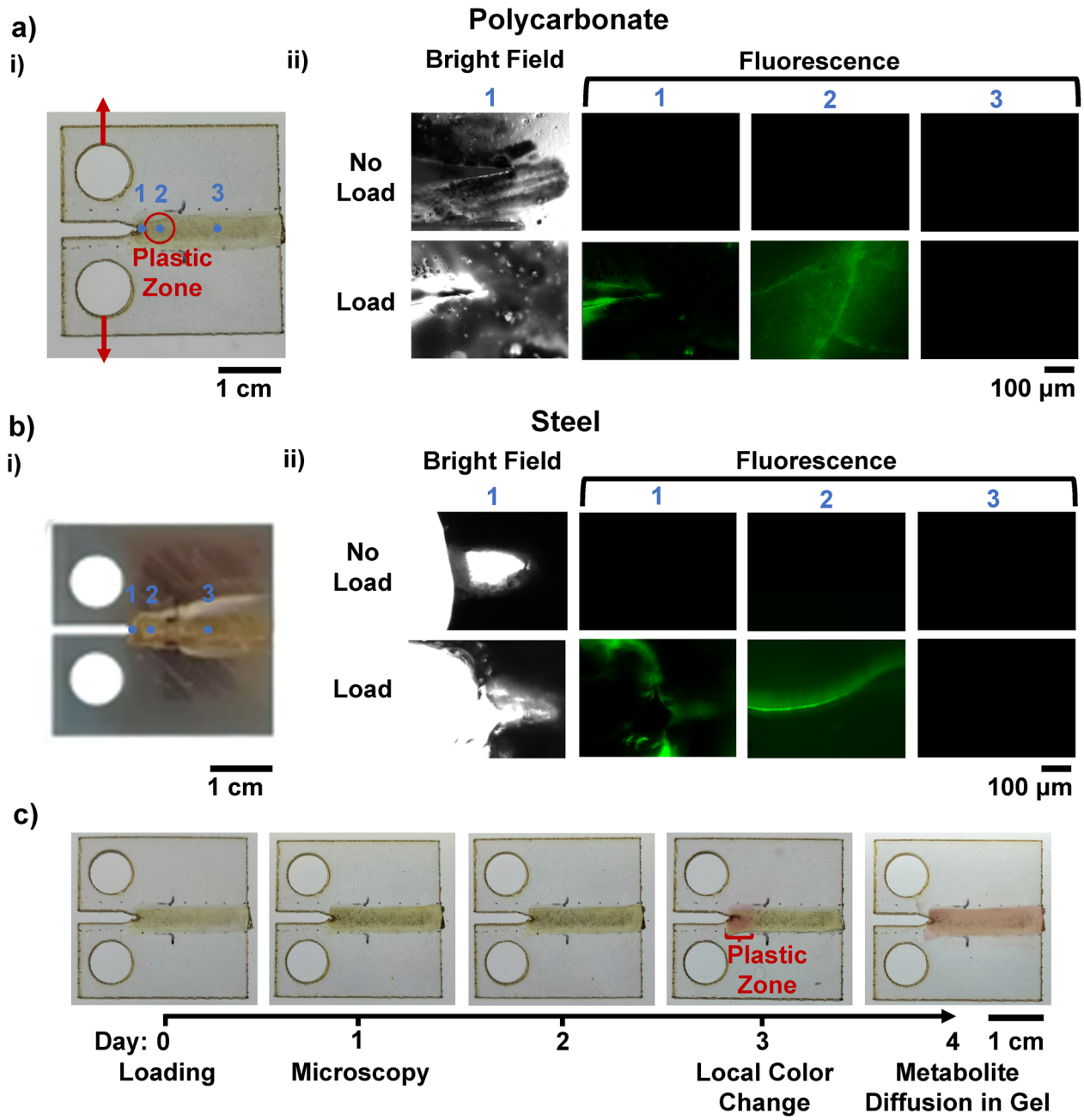

Fig. 5 Detection of crack propagation in compact tension specimens. (a) (i) Example image of a coated polycarbonate compact tension sample. Black lines denote grip boundaries and arrows indicate applied forces from the pins used to mount the sample. (a) (ii) Microscopy images at each position after 24 hours: (1) crack tip, (2) plastic zone, and (3) region far from the crack tip. Samples that underwent no loading did not show any crack growth and fluorescence. Samples loaded for 1 hour (shown here) showed substrate crack growth and fluorescence at the crack tip and plastic zone. Samples that were loaded for 3 hours (Fig. S22, SI) showed the largest substrate crack growth and also had fluorescent coating cracks in the plastic zone. (b) (i) A steel compact tension sample and (ii) microscopy images for crack detection. (c) The addition of the pH indicator, phenol red, enabled visual detection of the plastic region with substrate cracks after 3 days for bacterial growth post fatigue testing.

intermittent use of a part or structure; in this context a microbial growth timescale of 1 to 4 days to warn of impending damage is quite practical. Using the stress concentration geometry from above, we demonstrate in-situ detection of substrate plasticity due to intermittent fatigue loading. Samples were subjected to no loading, 1 × 1 hour, 3 × 1 hour, and 1 × 3 hours of cyclic loading of 0 N to 100 N tension, at 0.03 Hz (Fig. S16, SI) – the initial cycle of this loading corresponds to approximately 1% strain of the crosshead displacement. A custom *in situ* fluorescence imaging setup was used to monitor samples undergoing cyclic loading (Fig. 4b(i)). A statistically significant increase in fluorescence of the stress concentrated region *versus* the unstressed region was observed for the 3 × 1 hour loaded sample at 48 hours and for the 3 hour continuously loaded sample at 32 hours (Fig. 4b(ii)). These results were validated using microscopy imaging at 48 hours to check for cracks in the spore-PMMA layer (Fig. 4c). No coating cracks or fluorescence were observed in the spore-PMMA layer in the unloaded control sample. The sample loaded for 1 hour showed surface level damage *via* a branched pattern but no through cracks in the coating (Fig. S17, SI). Intensity scaled images of the control (uncracked) and cracked regions are provided in Fig. S18 (SI) to enable visual comparison of the different loading histories.

1.4 Response to deformation ahead of fatigue cracks in different structural materials for early detection

We demonstrate that our coating can detect regions of plasticity ahead of a propagating crack, critical for avoiding catastrophic failure. This might be useful to indicate where a material is likely to crack but also to enable repair prior to failure. A standard ASTM crack propagation geometry for the structural material, the compact tension specimen (Fig. S19, SI), was used for testing (note: our samples are thin and do not meet the typical plane strain version of this standard geometry). The samples contain a pre-crack made using a razorblade before coating. Samples were then coated along a narrow region covering the area where the crack was expected to propagate. The samples were then cyclically loaded for 1 hour (Fig. 5 and Fig. S20, SI) and 3 hours (Fig. S21, SI) (Fig. 5a(i)). The applied cyclic loading resulted in crack propagation on the order of hundreds of microns. Three regions of interest were imaged 24 hours after mechanical loading: the crack tip, the plastic zone just ahead of the crack tip, and a far field region where no cracks were expected, as annotated in Fig. 5a(i). Fluorescent cracks in the coating are observed at the crack tip and plastic zone for samples that were loaded from 0 N to 60 N, at 0.03 Hz, for 1 hour, indicating successful detection of plasticity ahead of the crack. The crack in the structural material was tracked *via* imaging during loading, while the coating cracks were examined *via* microscopy. All images for bright field and fluorescence of different loading conditions are included in Fig. S22 (SI). No cracks in the coating were observed for samples that underwent no loading or for the region far from the crack tip (Fig. 5a(ii)).

The coating also proved to be effective on a different structural material, demonstrating that the coating is not substrate chemistry specific. We coated and tested steel A572 compact tension specimens. A572 is a low alloy, high strength steel that is common in structural applications.[83,84] A razor blade was used to achieve a sharp pre-crack stress concentration of approximately 0.32 mm (Fig. S23, SI) to ensure that a crack propagated during loading (Fig. S24, SI). Fig. 5b(i) shows successful application of the coating to a steel compact tension sample. The steel crack propagation was approximately 200 μm, yet the crack and plastic zone deformation was successfully detected *via* the cell fluorescence (Fig. 5b(ii)). Steel detection images are included in Fig. S25 (SI), including the pre-coating and control samples.

One major benefit of including a biological component in material design is the potential to leverage the biological component for structural material crack mitigation strategies. Genetic engineering could be harnessed to use cells to mediate the crack environmental conditions, for example to promote crack blunting to prevent crack propagation.[5,85,86] To demonstrate this promise, we integrated a pH indicator, phenol red, into the nutrient layer, to demonstrate that the embedded cells in the coating can be used to alter the crack environment pH. A transparent polycarbonate compact tension sample was utilized rather than a steel specimen to facilitate visualization. Samples were first coated and cyclically loaded on Day 0 and then were imaged once a day to check for colorimetric changes due to pH shifts. A shift in the pH from approximately 7 to greater than 8 based on the color change was first observed at 3 days post testing, two days after crack detection *via* fluorescent microscopy (Fig. 5c). The delayed colorimetric shift is due to the need for significant bacterial proliferation to drive the change in pH through the production of metabolites or waste products. As expected, this initial color change occurs in the plastic zone. By the fourth day, the metabolites have diffused throughout the gel leading to color along the entire specimen width. No fluorescence or small cracks were observed in the far region on the fourth day, confirming that the global color change was indeed due to diffusion of metabolites from the bacterial growth in the plastic zone cracks. The additional colorimetric option for crack detection makes the coating more accessible for use without imaging equipment or genetic modification. A colorimetric change leads to a detection zone that enlarges spatially over time which can be used to infer the source, and demonstrates the potential of the coating to control the crack environment for future crack mitigation.

2 Conclusion

Early crack detection in structural materials is essential for safety critical applications and minimizing material waste. We created a hybrid living coating capable of sense-and-response behavior as often is observed in nature. Our coating successfully senses localized plasticity *in situ* and can be applied as a coating for different structural materials for detection of

deformation and the onset of fatigue cracks. The biohybrid coating also holds the potential to be harnessed for crack mitigation, by leveraging the biological component. Our coating might be suitable for use on internal surfaces, such as ship hulls, where crack detection and mitigation are particularly challenging. The outlined material selection process, including matrix and organism requirements, candidate selection, and comprehensive evaluation, will facilitate the development of other biohybrid composites to expand the field of living materials and increase material functionality. The coating successfully detects structural material plastic deformation associated with the onset and propagation of cracks, creating an ideal tool for *in situ* monitoring of fatigue that can be used for different geometries and materials. Our hybrid living material presents a major leap towards increasing material functionality and improving safety and sustainability through early crack detection preventing catastrophic failure. Future work is needed to explore coating performance under varied application relevant environmental conditions and even longer timescales and to harness the biological function for damage mitigation and self-healing.

3 Experimental section

3.1 Bacterial sporulation and culture conditions

We used a *B. subtilis* 168 trpC2 strain with genotype *sacA*::P*vegI-nfC* translation initiation region with AUUAUG start codons-3XFlag-GFP. Cells were grown in lysogeny broth (LB) Miller (VWR, Radnor, PA) at 37 °C on an orbital shaker (VWR) at 200 rotations per minute (rpm) unless otherwise noted. Plates were made using 1.5% bacteriological agar (VWR) and 2.5% LB Miller broth powder (VWR). All reagents were sourced from Sigma Aldrich (St. Louis, MO) unless otherwise noted. Spores were produced by first inoculating 4 mL of LB medium with *B. subtilis*. The bacteria were grown overnight at 37 °C at 200 rpm. The overnight culture was then diluted to an optical density (OD) at 600 nm of 0.1–0.2 in 10 ml LB. Cells were grown to an OD of 0.8 at 37 °C at 200 rpm before centrifuging the cells at 13 000×*g* for 1 minute, washing the pellet with 1 mL 1× phosphate buffered saline (PBS) (VWR), and re-suspending the pellet in 5 mL Difco Sporulation Medium (DSM). DSM broth consisted of 8 g nutrient broth, 1 g potassium chloride, 1 mL magnesium sulfate (1 M), 1 mL manganese chloride (10 mM), 1000 mL deionized water, 0.5 mL calcium chloride (1 M stock concentration), and 1 mL iron sulfate (1 M stock concentration). After 24 hours of growth in DSM media, the cells were treated with 1 mg mL^{-1} lysozyme for 1 hour at room temperature. The cells were subsequently washed 6 times with 1× PBS, lyophilized overnight and stored at 4 °C.

3.2 Spore growth and fluorescence testing

To compare spore growth and fluorescence between commercially available *B. subtilis* spores (Ecosh Life, Estonia) and the spores produced through the outlined sporulation protocol using the strain with GFP expression, 200 μl of LB were inoculated with 1 mg of spores from non-fluorescent and fluorescent cell lines on a 96-well plate. Tests were performed in triplicate. The optical density at 600 nm (Fig. S1a, SI) and fluorescence at an excitation and emission of 488 and 509 nm (Fig. S1b and c, SI) respectively were measured at 0 hours and at 22 hours. A blank well with just LB was used as a control for background signal.

3.3 Fabrication of additional matrix polymer candidates for the spore-polymer composite

Polymer matrix materials that were considered for the spore-polymer composite, include epoxy, polyethylmethacrylate (PEMA), tetra(ethylene glycol) diacrylate (TetEGDA) and PMMA. Epoxy 4500 was mixed with the curing agent 4570 from Fiber Glast (Brockville, OH) at a ratio of 100 : 22 and allowed to cure for 14 hours overnight at 65 °C as per the manufacturer's guidelines. TetEGDA and PEMA (Polysciences Inc., Warrington, PA) were made by mixing the monomer, tetraethylene glycol diacrylate or ethyl methacrylate respectively, with 1% 2-hydroxy-2-methylpropiophenone initiator and curing for 30 minutes under UV. PMMA was made by mixing MMA with 1% 2-hydroxy-2-methylpropiophenone initiator and curing for approximately 50 minutes under UV until the polymer was fully solidified.

3.4 Cytotoxicity test

Cytotoxicity tests were conducted to determine which polymer matrix material candidates were biocompatible with spore germination and cell growth. *B. subtilis* spores were first bead plated on LB-agar gel plates. Three polymer blocks, approximately 1 cm × 1 cm × 1 cm, for each of the material candidates were then placed on the plates. The plates were incubated at 37 °C for 24 hours and imaged following the growth period. Cytotoxic materials lead to a ring of no growth on the agar surrounding the block following the growth period. The diameter of the ring of no growth was measured to quantify the material's toxicity. The width of the block was subtracted from the diameter of the growth ring and divided by two to determine the size of the growth inhibition zone.

3.5 Embedded spore revivability test

PMMA was tested for whether spores could be revived once embedded in the material by mixing in spores with the selected polymers and testing growth. Small blocks of polycarbonate (Robosource, Worcester, MA) were first cut to act as the structural material. Spores and methylmethacrylate were then mixed at a 1% w/v ratio and cured to coat the polycarbonate blocks. A layer of PMMA with no spores was finally cured on top to ensure that all spores were coated with the polymer. The blocks were then put in LB growth media for 24 hours. The optical density of the media at 600 nm was measured each hour for 24 hours to quantify growth. Three groups were considered: a polymer coated block with no spores in the coating, an intact spore-polymer coated block, and a cracked spore-polymer coated block.

3.6 Fabrication of polycarbonate samples and coating with spore-PMMA layer

Polycarbonate (Robosource, Worcester, MA) sheets were cut into dog bone shapes with a miter saw following the ASTM D638 Type 5 standard with a gauge length of 25.4 mm and sanded to remove any uneven edges. To make the selected coating, MMA was mixed with 1% 2-hydroxy-2-methylpropiophenone (TCI America, Portland, OR) initiator and pre-cured for 40 minutes under a 6-watt UV-A lamp (VWR) at a wavelength of 365 nm. A 1% w/v mixture of spores to the volume of partially cured PMMA was made. The spore-PMMA mixture was gently pipetted up and down to evenly mix in the spores until visually homogeneous. Any inhomogeneities were vortexed to ensure a fully uniform spore dispersion. A 1% w/v solution of spores ensures effective spore coverage throughout the coating without affecting mechanical properties, such as stiffness (SI, Fig. S4). The mixture was then pipetted onto the structural substrate to form a coating. The sample was exposed to an additional 30 minutes of UV to fully solidify the coating. A second layer of pre-cured PMMA was applied, fully covering the first layer, and cured for 30 minutes to ensure that no spores were exposed at the coating surface. The final coating had an average thickness of 0.28 ± 0.10 mm with each layer of PMMA approximately equal in thickness. Both spore and non-spore (control) samples received the second coat for consistency. Polycarbonate dog bone circular stress concentration and compact tension samples were coated following the same procedure.

3.7 Fabrication of polyacrylamide nutrient gel

The nutrient layer was made from polyacrylamide (pAAM) gel based on the protocol outlined by Tuson *et al*.[87] To produce the gel, 710.8 mg of acrylamide (Sigma Aldrich) and 30.834 mg methylene bis-acrylamide (MBA) (Sigma Aldrich) were dissolved in 10 mL of deionized water. The solution was filter sterilized using a Steriflip-GP, 0.22 μm, polyethersulfone, gamma irradiated filter (EDM Milipore, Burlington, MA). Following sterilization, 10 μL of *N*,*N*,*N*′,*N*-Tetramethyl ethylenediamine (TEMED) (Oakwood Chemical, Estill, SC) and 10 mg of ammonium persulfate (APS) (Sigma Aldrich) were added before pouring the solution into ASTM D638 Type 5 dog bone shaped Teflon molds for mechanical tests or Petri dishes for growth tests or layers for samples. A mold required 0.5 mL of solution and a 55 mm diameter Petri dish (VWR) used 10 mL solution. The gels were then cured at 45 °C for 60 min. After curing, gels were soaked in a 1 L bath of deionized water over night for three days with the water renewed each day to remove uncured monomers as per the protocol outlined by Tuson *et al*. The gels were then soaked in LB solution for 24 hours to infuse nutrients for bacterial growth and sterilized using a UV Stratalinker (REUZEit, Temecula, CA) with 3000 × 100 μJ energy mode to ensure no live cells were present in the nutrient gels.

3.8 Fabrication of additional nutrient gel candidates

Several gels were considered to serve as the nutrient layer including LB-agar, LB-agarose, LB-pAAM-alginate, calcium-alginate, and LB-pAAM (described in previous section). LB-agar gel was made by dissolving 2.5 g LB powder (VWR) and 1.5 g bacteriological grade agar (VWR) in 100 ml deionized water and autoclaving to sterilize before pouring plates to test growth or filling dog bone molds for tensile testing. LB-agarose was made by mixing 1% agarose (Sigma Aldrich) in deionized water and casting the mixture in a plate or dog bone form. The plates were sterilized under UV using 3000 μJ with a Stratalinker. To produce an LB-agarose plate, LB medium was used instead of water. LB-pAAM-alginate was made with 10 mL LB broth, 0.72 g acrylamide, 0.0036 g *N*,*N*-Methylbis (acrylamide), and 0.072 g potassium persulfate initiator, and 0.024 g sodium alginate (all chemicals from Sigma Aldrich unless otherwise indicated). Calcium-alginate gels were produced by mixing 5% sodium alginate in deionized water and stirring over night to allow for bubbles to escape to form a homogeneous solution. The gel was then solidified by soaking it in 1 M calcium chloride (Sigma Aldrich) solution.

3.9 Water loss assay

To test water loss, pAAM gel was cast in 5.5 cm diameter Petri dishes and covered with the desired candidate material for preventing water loss and left uncovered at a temperature of 23 °C and 30% humidity. The plate was weighed on a scale (LA2002E, Metlier Toledo, Columbus, OH) initially and on each subsequent day. The percent water loss was calculated to determine the effectiveness of various materials for preventing water loss in the gel. The weight was corrected to discount the weight of the Petri dish.

3.10 Fabrication of polycarbonate samples with complete coating

Fabrication of polycarbonate samples with the complete coating initially followed the procedure described in ''Fabrication of Polycarbonate Samples and Coating with spore-PMMA Layer''. Nutrient gel layer strips were cut and layered onto the spore-PMMA coated samples and sealed to prevent water loss with silicone (SS-155 UV Dual Cure Silicone Adhesive Sealant – Humiseal 1C63 Offset, silicone solutions, Cuyahoga Falls, OH). The silicone layer was cured under UV for approximately 1 hour and given 24 hours to set before sample use.

3.11 Tensile testing

We conducted uniaxial tensile testing to determine the mechanical properties of each material candidate when selecting the matrix material, to check if the coating layered on polycarbonate altered mechanical properties, and to test the coating performance when subjected to different amounts of strain. Specimens followed the ASTM D638 Type 5 standard shape with a gauge length of 25.4 mm. Tests were conducted on a Zwick-Roell (Zwick Roell, Germany) Z010 system with a 10 000 N capacity load cell. A constant crosshead displacement rate of 0.05 mm s^{-1} was applied corresponding roughly to a strain rate of 0.002 s^{-1}, determined by dividing the crosshead displacement rate by the gauge length. Strain was determined by dividing the final crosshead displacement by the initial

gauge length. A 20 N load cell was used for tensile testing of freestanding gels. Three replicates were conducted for each material. All stress values are reported as engineering stress and were calculated using the initial cross-sectional area of the sample.

3.12 Fabrication of dog bone samples containing stress concentrations for fatigue testing

Fatigue testing following testing protocols (ASTM D 5045-99) and the Standard Test Method for Open-Hole Tensile Strength of Polymer Matrix Composite Laminates (ASTM 5766) was conducted to determine the effectiveness of the coating for detecting fatigue cracking. Dog bone shaped specimens were laser cut using a Boss Laser LS-2440 (Boss Laser, Sanford, FL) at 60% power, a speed of 20 mm s^{-1}, and a single pass following the dimensions outlined in the relevant ASTM standard. The thickness of 1/32″ polycarbonate was used to enable laser cutting of the samples.

3.13 Digital image correlation

Digital image correlation (DIC) analysis was conducted with a Point Grey camera (GRAS-50S5M-C, Richmond, Canada) with a 12x zoom lens (Navitar, Rochester, NY). A speckle pattern was applied to the dog bone samples containing circular stress concentrations, with matte white spray paint (Fusion, Cleveland, OH). Imaging was carried out using VIC-Snap 8 software and analyzed using VIC-2D Digital Image Correlation (Correlated Solutions, Irmo, SC). An imaging rate of 15 frames s^{-1} was used for DIC tests.

3.14 *In situ* fluorescence imaging

A fluorescence setup was assembled to image full field fluorescence during mechanical testing. The setup consisted of a UV light, filter, and camera. A UV light at at wavelength of 395 nm (WF-502B, Ultrafire, Chicago, IL) was used to excite the sample. A Point Grey (GRAS-50S5M-C) camera with a 525 nm microscope filter in front of the lens was used to image the sample. ImageJ software was used to conduct fluorescent image analysis. Images were taken of the regions of high and low stress surrounding the circular stress concentration. The average fluorescence intensity was measured in ImageJ and recorded for the in-frame sample area, which was kept consistent between time points.[88]

3.15 Compact tension testing

Polycarbonate compact tension testing samples were lasercut at 60% power, a speed of 20 mm s^{-1}, and a single pass and following the standard dimensions provided by ASTM 3999 (Fig. S19, SI). Polycarbonate sheets with a thickness of 1/32″ were used, resulting in a plane stress case according to ASTM E399. Custom grips were machined using tool steel to mount the samples to the Zwick Roell load frame. Polycarbonate samples were pre-cracked to a depth of 1 mm using a single swipe with a steel razor blade, as per ASTM guidelines, before coating. Coated polycarbonate samples were loaded from 0 to 75 N, at 0.03 Hz for 0 hours, 1 hour, and 3 hours.

Steel samples were water jet cut from stainless steel A572 following the same dimensions used for polycarbonate compact tension samples. Steel samples were pre-cracked using the razor blade method with an average pre-crack value of 0.32 mm. Steel compact tension tests were conducted from 0 to 200 N, at 0.05Hz for 360 cycles. Both polycarbonate and steel samples were imaged at a rate of 5 images per cycle for the duration of testing to track the crack growth. Images were analyzed using ImageJ to make accurate crack length measurements, that aided in distinguishing cracks in the structural material from coating cracks in the plastic zone. Samples were imaged using microscopy (Leica DMi8 C microscope) at 24 hours after the start of loading to measure fluorescence response.

3.16 Change in pH in crack environment

Additional tests were done to demonstrate changes in the crack pH through the addition of phenol red indicator which turns bright pink at an approximate pH value of 8. The indicator was added to the initial LB used to infuse the pAAM nutrient layer. A phenol red stock concentration of 15 mg mL^{-1} in deionized water was used to make a final phenol red concentration of 1 μL mL^{-1} in the LB solution. The sample was then subjected to fatigue loading and imaged each day to observe any color changes due to bacterial production of metabolites.

3.17 Spontaneous germination testing

To ensure that samples do not spontaneously germinate, fully coated samples were stored in a humidity chamber (Associated Environmental Systems, Ayer, MA) at 25 °C, 95% humidity. Three samples were removed each week for microscopy imaging for 4 weeks to check for any fluorescence or cell growth.

3.18 Microscopy

Fluorescence and optical microscopy were used to visualize crack patterns and cell fluorescence. A Leica DMi8 C microscope (Leica, Germany) was used with 20× magnification, 5 ms exposure, and gain of 10. A 488 nm excitation wavelength and a 530/40 nm emission filter were used for fluorescence measurements.

Author contributions

Conceptualization, E. W. v. W., A. G., M. N. S.; data curation, E. W. v. W., T. C.; formal analysis, E. W. v. W.; writing – original draft preparation, E. W. v. W.; writing – review and editing, E. W. v. W., T. C., I. L. B., A. G., M. N. S.; visualization, E. W. v. W.; supervision, I. L. B., M. N. S.; project administration, M. N. S.; funding acquisition, N. B., A. G., M. N. S. All authors have read and agreed to the published version of the manuscript.

Conflicts of interest

There are no conflicts to declare.

Data availability

The data supporting this article have been included as part of the supplementary information (SI) and are available *via* Zenodo at https://doi.org/10.5281/zenodo.15855717.[89] Supplementary information includes spore growth curves, material selection trials, supporting figures for design of nutrient gel layer and all imagines for localized fatigue, polycarbonate, and steel tests. See DOI: https://doi.org/10.1039/d5ma01053e.

Acknowledgements

We thank Professor Heather Feaga's lab at Cornell University for providing fluorescent *B. subtilis* strains.[90,91] We also thank Professor Charles Diesendruck at the Technion Israel Institute of Technology, for recommendations for polymer synthesis and molding of samples. This work was supported through the NSERC CGS-D scholarship (E. W. v. W.). This publication is based in part on work supported by the US Department of the Navy, Office of Naval Research (Grant Award No. N000142412479). This work was supported and performed in part at the Engineered Living Materials Institute. This work was performed in part at the Cornell NanoScale Facility, a member of the National Nanotechnology Coordinated Infrastructure (NNCI), which is supported by the National Science Foundation (Grant NNCI69 2025233).

References

1 S. Suresh, Fatigue of materials, *Adv. Mater.*, 1992, **5**(4), 309, DOI: 10.1002/adma.l9930050420.
2 A. Wohler, Uber die festigkeitsversuche mit eisen und stahl, *ZfBw*, 1870, **20**, 73–106.
3 A. A. Griffith and G. I. Taylor, The phenomena of rupture and flow in solids, *Philos. Trans. R. Soc., A*, 1921, **221**(582), 163–198, DOI: 10.1098/rsta.l921.0006.
4 P. Paris, M. Gomez and W. Anderson, A rational an-alytic theory of fatigue, *Trend Eng.*, 1961, **13**, 9–14.
5 L. G. Bland and J. S. Warner Locke, Chemical and electrochemical conditions within stress corrosion and corro-sion fatigue cracks, *npj Mater. Degrad.*, 2017, **1**(1), 1–8, DOI: 10.1038/S41529-017-0015-0.
6 A. K. Vasudevan and K. Sadananda, Classification of environmentally assisted fatigue crack growth behavior, *Int. J. Fatigue*, 2009, **31**(11), 1696–1708, DOI: 10.1016/j.ijfatigue.2009.03.019.
7 J. Chen, F. Lin, D. Guo, T. Tang, Y. Miao, Y. Wu, W. Zhai, H. Huang, Z. Chi, Y. Chen and Z. Yang, *In situ* reversible and robust mechano-responsive ultralong phosphorescence of polyurethane elastomer, *Adv. Mater.*, 2024, **36**(50), 2409642, DOI: 10.1002/adma.202409642.
8 X. Ou, J. Pan, Q. Liu, Y. Niu, Y. Zhou and F. Yan, High-toughness C02-sourced ionic polyurea ad-hesives, *Adv. Mater.*, 2024, **36**(16), 2312906, DOI: 10.1002/adma.202312906.
9 S. Abbasi, R. B. Ladani, C. H. Wang and A. P. Mouritz, Improving the delamination fatigue resistance of composites by 3d woven metal and composite z-filaments, *Composites, Part A*, 2021, **147**, 106440, DOI: 10.1016/j.compositesa.2021.106440.
10 Z. Shaterian, A. K. Horestani, F. Martín and M. Mrozowski, Design of novel highly sensitive sensors for crack detection in metal surfaces: theoretical foundation and ex-perimental validation, *Sci. Rep.*, 2023, **13**(1), 18540, DOI: 10.1038/S41598-023-45556-8.
11 C. T. Anderson and J. J. Kieber, Dynamic construction, perception, and remodeling of plant cell walls, *Annu. Rev. Plant Biol.*, 2020, **71**, 39–69, DOI: 10.1146/annurev-arplant-081519-035846.
12 S. Bolamperti, I. Villa and A. Rubinacci, Bone remodeling: an operational process ensuring survival and bone mechanical competence, *Bone Res.*, 2022, **10**(1), 1–19, DOI: 10.1038/s41413-022-00219-8.
13 S. Wang and M. W. Urban, Self-healing polymers, *Nat. Rev. Mater.*, 2020, **5**(8), 562–583, DOI: 10.1038/S41578-020-0202-4.
14 H. M. Jonkers, A. Thijssen, G. Muyzer, O. Copuroglu and E. Schlangen, Application of bacteria as self-healing agent for the development of sustainable concrete, *Ecol. Eng.*, 2010, **36**(2), 230–235, DOI: 10.1016/j.ecoleng.2008.12.036.
15 S. R. White, N. R. Sottos, P. H. Geubelle, J. S. Moore, M. R. Kessler, S. R. Sriram, E. N. Brown and S. Viswanathan, Autonomic healing of polymer composites, *Nature*, 2001, **409**(6822), 794–797, DOI: 10.1038/35057232.
16 M. J. Robb, W. Li, R. C. R. Gergely, C. C. Matthews, S. R. White, N. R. Sottos and J. S. Moore, A robust damage-reporting strategy for polymeric materials enabled by aggregation-induced emission, *ACS Cent. Sci.*, 2016, **2**(9), 598–603, DOI: 10.1021/acscentsci.6b00198.
17 K. S. Toohey, N. R. Sottos, J. A. Lewis, J. S. Moore and S. R. White, Self-healing materials with microvascular networks, *Nat. Mater.*, 2007, **6**(8), 581–585, DOI: 10.1038/nmatl934.
18 A. P. Esser-Kahn, P. R. Thakre, H. Dong, J. F. Patrick, V. K. Vlasko-Vlasov, N. R. Sottos, J. S. Moore and S. R. White, Three-dimensional microvascular fiber-reinforced composites, *Adv. Mater.*, 2011, **23**(32), 3654–3658, DOI: 10.1002/adma.201100933.
19 J. F. Patrick, K. R. Hart, B. P. Krull, C. E. Diesendruck, J. S. Moore, S. R. White and N. R. Sottos, Continuous self-healing life cycle in vascularized structural composites, *Adv. Mater.*, 2014, **26**(25), 4302–4308, DOI: 10.1002/adma.201400248.
20 H. Cai, Z. Wang, N. W. Utomo, Y. Vidavsky and M. N. Silberstein, Highly stretchable ionically crosslinked acrylate elastomers inspired by polyelec-trolyte complexes, *Soft Matter*, 2022, **18**(39), 7679–7688, DOI: 10.1039/D2SM00755J.
21 C. Tang, L. Wang, J. Sun, G. Chen, J.-F. Shen, L. Wang, Y. Han, J. Luo, Z. Li, P. Zhang, S. Zeng, D. Qi, J. Geng, J. Liu and Z. Dai, Degradable living plastics programmed by engineered spores, *Nat. Chem. Biol.*, 2024, 1–6, DOI: 10.1038/S41589-024-01713-2.
22 H. S. Kim, M. H. Noh, E. M. White, M. V. Kandefer, A. F. Wright, D. Datta, H. G. Lim, E. Smiggs, J. J. Locklin, M. A. Rahman, A. M. Feist and J. K. Pokorski, Biocomposite

thermoplastic polyurethanes containing evolved bacterial spores as living fillers to facilitate polymer disintegration, *Nat. Commun.*, 2024, **15**(1), 3338, DOI: 10.1038/s41467-024-47132-8.

23 C. Gilbert and T. Ellis, Biological engineered living materials: Growing functional materials with genetically programmable properties, *ACS Synth. Biol.*, 2019, **8**(1), 1–15, DOI: 10.1021/acssynbio.8b00423.

24 S. Molinari, R. F. Tesoriero, D. Li, S. Sridhar, R. Cai, J. Soman, K. R. Ryan, P. D. Ashby and C. M. Ajo-Franklin, A de novo matrix for macroscopic living materials from bacteria, *Nat. Commun.*, 2022, **13**(1), 5544, DOI: 10.1038/s41467-022-33191-2.

25 L. Rivera-Tarazona, M. S. Kalairaj, T. Corazao, M. Javed, P. Zimmem, S.-R. Subashchandrabose and T. Ware, Controlling shape morphing and cell release in engineered living materials, *Biomater. Adv.*, 2022, **143**, 213182, DOI: 10.1016/j.bioadv.2022.213182.

26 L. L. Xiong, M. A. Garrett, J. A. Komfield and M. G. Shapiro, Living material with temperature-dependent light absorption, *Adv. Sci.*, 2023, **10**(30), 2301730, DOI: 10.1002/advs.202301730.

27 H. Mohsenin, R. Schmachtenberg, S. Kem-mer, H. J. Wagner, M. Johnston, S. Madlener, C. Dincer, J. Timmer and W. Weber, Signal-amplifying biohybrid material circuits for CRISPR/cas-based single-stranded RNA detection, *Adv. Mater. Technol.*, 2025, **10**(2), 2400981, DOI: 10.1002/admt.202400981.

28 E. W. van Wijngaarden, S. Bratcher, K. J. Lewis and C. J. Hernandez, Solute transport in engineered living materials using bone-inspired microscale channel networks, *Adv. Eng. Mater.*, 2023, **25**(24), 2301032, DOI: 10.1002/adem.202301032.

29 C. M. Heveran, R. Gerlach, C. J. Hernandez, K. Intemann, A. S. Meyer, C. Ajo-Franklin, M. Charrier, W. V. Srubar, N. Joshi, A. Nelson and M. W. Fields, Unlocking the societal potential of engineered living materials, *Matter*, 2024, **7**(9), 2846–2858, DOI: 10.1016/j.matt.2024.07.011.

30 S. Molinari, R. P. Tesoriero and C. M. Ajo-Franklin, Bottom-up approaches to engineered living materials: Challenges and future directions, *Matter*, 2021, **4**(10), 3095–3120, DOI: 10.1016/j.matt.2021.08.001.

31 P. Q. Nguyen, N.-M. Dorval Courchesne, A. Duraj-Thatte, P. Praveschotinunt and N. S. Joshi, Engineered living materials: Prospects and challenges for using biological systems to direct the assembly of smart materials, *Adv. Mater.*, 2018, **30**(19), 1704847, DOI: 10.1002/adma.201704847.

32 A. Koshti, Assessment of dye penetrant crack detectability in external corners using similarity analysis, in *Nondestructive Characterization and Monitoring of Advanced Material, Aerospace, Civil Infrasttucture, and Transportation XII*, vol. 10599, 2018.

33 H. Kaveh and R. Alhajj, Recent advances in crack detection technologies for structures: a survey of 2022-2023 literature, *Front. Built. Environ.*, 2024, **10**, 1321634, DOI: 10.3389/fbuil.2024.1321634.

34 H. S. Munawar, A. W. A. Hammad, A. Haddad, C. A. Pereira Soares and S. T. Waller, Image-based crack detection methods: A review, *Infrastructures*, 2021, **6**(8), 115, DOI: 10.3390/infrastructures6080115.

35 V. Belloni, A. Sjolander, R. Ravanelli, M. Crespi and A. Nascetti, Crack monitoring from motion (CMfM): Crack detection and measurement using cam eras with non-fixed positions, *Autom. Constr.*, 2023, **156**, 105072, DOI: 10.1016/j.autcon.2023.105072.

36 J. Zhang, G. Y. Tian and A. B. Zhao, Passive RFID sensor systems for crack detection & characterization, *NDT Int.*, 2017, **86**, 89–99, DOI: 10.1016/j.ndteint.2016.11.002.

37 C. J. Stull, C. J. Earls and P.-S. Koutsourelakis, Model-based structural health monitoring of naval ship hulls, *Comput. Methods Appl. Mech. Eng.*, 2011, **200**(9), 1137–1149, DOI: 10.1016/j.cma.2010.11.018.

38 A. Silva-Campillo, F. Perez-Arribas and J. C. Suarez-Bermejo, Health-monitoring systems for marine structures: A review, *Sensors*, 2023, **23**(4), 2099, DOI: 10.3390/S23042099.

39 Y. Yao and B. Glisic, Detection of steel fatigue cracks with strain sensing sheets based on large area electronics, *Sensors*, 2015, **15**(4), 8088–8108, DOI: 10.3390/S150408088.

40 R. Wang, Q. Wu, F. Yu, Y. Okabe and K. Xiong, Nonlinear ultrasonic detection for evaluating fatigue crack in metal plate, *Struct. Health Monit.*, 2019, **18**(3), 869–881, DOI: 10.1177/1475921718784451.

41 J. Zhang, G. Yun Tian, A. M. J. Marindra, A. I. Sunny and A. B. Zhao, A review of passive RFID tag antenna-based sensors and systems for structural health monitoring applications, *Sensors*, 2017, **17**(2), 265, DOI: 10.3390/sl7020265.

42 P. Duffour, M. Morbidini and P. Cawley, A study of the vibro-acoustic modulation technique for the detection of cracks in metals, *J. Acoust. Soc. Am.*, 2006, **119**, 1463–1475, DOI: 10.1121/l.2161429.

43 R. Miorelli, C. Reboud, D. Lesselier and T. Theodoulidis, Eddy current modeling of narrow cracks in planar-layered metal structures, *IEEE Trans. Magn.*, 2012, **48**(10), 2551–2559, DOI: 10.1109/TMAG.2012.2197403.

44 S. Deif and M. Daneshmand, Multiresonant chip-less RFID array system for coating defect detection and corrosion prediction, *IEEE Trans. Ind. Electron.*, 2020, **67**(10), 8868–8877, DOI: 10.1109/TIE.2019.2949520.

45 G. Li, D. Lan, X. Zheng, X. Li and J. Zhou, Automatic pavement crack detection based on single stage salient-instance segmentation and concatenated feature pyramid network: International journal of pavement engineering, *Int. J. Pavement Eng.*, 2020, **23**(12), 4206–4222, DOI: 10.1080/10298436.2021.1938045.

46 S. Dey, O. Salim, H. Masoumi and N. C. Karmakar, A novel UHF RFID sensor based crack detection technique for coal mining conveyor belt, *IEEE J. Radio Freq. Identif.*, 2022, **6**, 19–30, DOI: 10.1109/JRFID.2021.3098624.

47 Y. Vidavsky, S. J. Yang, B. A. Abel, I. Agami, C. E. Diesendruck, G. W. Coates and M. N. Silberstein, Enabling room-temperature mechanochromic activation in a glassy polymer: Synthesis and characterization of

spiropyran polycarbonate, *J. Am. Chem. Soc.*, 2019, **141**(25), 10060–10067, DOI: 10.1021/jacs.9b04229.

48 A.-D. N. Celestine, B. A. Beiermann, P. A. May, J. S. Moore, N. R. Sottos and S. R. White, Fracture-induced activation in mechanophore-linked, rubber toughened PMMA, *Mymer*, 2014, **55**(16), 4164–4171, DOI: 10.1016/j.polymer.2014.06.019.

49 N. Deneke, M. L.ăRencheck and C. S.ăDavis., An engineer's introduction to mechanophores, *Soft Matter*, 2020, **16**(27), 6230–6252, DOI: 10.1039/D0SM00465K.

50 E. M. Nofen, N. Zimmer, A. Dasgupta, R. Gunckel, B. Koo, A. Chattopadhyay and L. L. Dai, Stress-sensing thermoset polymer networks *via* grafted cinnamoyl/cyclobutane mechanophore units in epoxy, *Polym. Chem.*, 2016, **7**(47), 7249–7259, DOI: 10.1039/C6PY01463A.

51 C. A. Jones, N. L. Padula and P. Setlow, Effect of mechanical abrasion on the viability, disruption and germination of spores of bacillus subtilis, *J. Appl. Microbiol.*, 2005, **99**(6), 1484–1494, DOI: 10.1111/j.l365-2672.2005.02744.x.

52 E. Black, P. Setlow, A. Hocking, C. Stewart, A. Kelly and D. Hoover, Response of spores to high-pressure processing, *Compr. Rev. Food Sci. Food Saf.*, 2007, **6**(4), 103–119, DOI: 10.1111/j.l541-4337.2007.00021.x.

53 P. Setlow, S. Wang and Y.-Q. Li, Germination of spores of the orders bacillales and clostridiales, *Annu. Rev. Microbiol.*, 2017, **71**, 459–477, DOI: 10.1146/annurev-micro-090816-093558.

54 P. Setlow, Spore resistance properties, in *The Bacterial Spore*, John Wiley & Sons, Ltd, 2016, pp. 201–215. ISBN 978-1-68367-078-0.

55 F. Lyu, T. Zhang, M. Gui, Y. Wang, L. Zhao, X. Wu, L. Rao and X. Liao, The underlying mechanism of bacterial spore germination: An update review, *Compr. Rev. Food Sci. Food Saf.*, 2023, **22**(4), 2728–2746.

56 Y. Gao, J. D. Amon, L. Artzi, F. H. Ramirez-Guadiana, K. P. Brock, J. C. Cofsky, D. S. Marks, A. C. Kruse and D. Z. Rudner, Bacterial spore germination receptors are nutrient-gated ion channels, *Science*, 2023, **380**(6643), 387–391, DOI: 10.1126/science.adg9829.

57 J. D. Amon, L. Artzi and D. Z. Rudner, Genetic evidence for signal transduction within the bacillus subtilis GerA germinant receptor, *J. Bacteriol.*, 2022, **204**(2), e00470–21, DOI: 10.1128/jb.00470-21.

58 M. Paidhungat and P. Setlow, Isolation and characterization of mutations in bacillus subtilis that allow spore germination in the novel germinant d-alanine, *J. Bacteriol.*, 1999, **181**(11), 3341–3350, DOI: 10.1128/jb.l81.11.3341-3350.1999.

59 C. Zhong, Spores hit the spot, *Nat. Chem. Biol.*, 2020, **16**(2), 108–109, DOI: 10.1038/s41589-019-0451-y.

60 N. Koopman, L. Remijas, J. Seppen, P. Set-low and S. Brul, Mechanisms and applications of bacterial sporulation and germination in the intestine, *Int. J. Mol. Sci.*, 2022, **23**(6), 3405, DOI: 10.3390/ijms230634O5.

61 M. Bagga, C. Hamley-Bennett, A. Alex, B. L. Freeman, I. Justo-Reinoso, L. C. Mihai, S. Gebhard, K. Paine, A. D. Jefferson, E. Masoero and I. D. Ofieru, Advancements in bacteria based self-healing concrete and the promise of modelling, *Constr. Build. Mater.*, 2022, **358**, 129412, DOI: 10.1016/j.conbuildmat.2022.129412.

62 H. W. Kua, S. Gupta, A. N. Aday and W. V. Srubar, Biochar-immobilized bacteria and superab-sorbent polymers enable self-healing of fiber-reinforced concrete after multiple damage cycles, *Cem. Concr. Compos.*, 2019, **100**, 35–52, DOI: 10.1016/j.cemconcomp.2019.03.017.

63 W. Pungrasmi, J. Intarasoontron, P. Jongvivatsakul and S. Likitlersuang, Evaluation of microencapsulation techniques for MICP bacterial spores applied in self-healing concrete, *Sci. Rep.*, 2019, **9**(1), 12484, DOI: 10.1038/S41598-019-49002-6.

64 H.-W. Reinhardt and M. Jooss, Permeability and self-healing of cracked concrete as a function of temperature and crack width, *Cem. Concr. Res.*, 2003, **33**(7), 981–985, DOI: 10.1016/S0008-8846(02)01099-2.

65 M. Peplow, Bioconcrete presages new wave in environmentally friendly construction, *Nat. Biotechnol.*, 2020, **38**(7), 776–778, DOI: 10.1038/s41587-020-0595-z.

66 E. Bremer, A. Calteau, A. Danchin, C. Harwood, J. D. Helmann, C. Medigue, B. O. Palsson, A. Sekowska, D. Vallenet, A. Zuniga and C. Zuniga, A model industrial workhorse: Bacillus subtilis strain 168 and its genome after a quarter of a century, *Microb. Biotechnol.*, 2023, **16**(6), 1203–1231, DOI: 10.1111/1751-7915.14257.

67 X. Zhang, A. Al-Dossary, M. Hussain, P. Set-low and J. Li, Applications of bacillus subtilis spores in biotechnology and advanced materials, *Appl. Environ. Microbiol.*, 2020, **86**(17), e01096–20, DOI: 10.1128/AEM.01096-20.

68 Marine coating performance ten year report, 1988.

69 S. Chaudhary. Bio-based UV-curable films and the effect of bio-content on the properties of the films, 2022.

70 X. Liu, S. Veldhuis, R. Mathews and I. Zhitomirsky, Dip coating of poly(ethyl methacrylate) and composites from solutions in isopropanol-water co-solvent, *Colloids Surf., A*, 2021, **631**, 127703, DOI: 10.1016/j.colsurfa.2021.127703.

71 P. Domachuk, K. Tsioris, F. G. Omenetto and D. L. Kaplan, Biomicrofluidics: Biomaterials and biomimetic designs, *Adv. Mater.*, 2010, **22**(2), 249–260, DOI: 10.1002/adma.200900821.

72 S. M. Pituru, M. Greabu, A. Totan, M. Imre, M. Pantea, T. Spinu, A. M. C. Tancu, N. Olivia Popoviciu, L.-I. Stanescu and E. Lonescu, A review on the biocompatibility of PMMA-based dental materials for interim prosthetic restorations with a glimpse into their modem manufacturing techniques, *Material*, 2020, **13**(13), 2894, DOI: 10.3390/mal3132894.

73 O. F. Farag, N. A. M. Eid and E. M. AbdelFattah, Understanding the impact of plasma functionalized MWCNTs on the structure, physicochemical and mechanical properties of PEMA, *Sci. Rep.*, 2025, **15**(1), 4755, DOI: 10.1038/S41598-025-88246-3.

74 S. Ramanathan, Y.-C. Lin, S. Thimmurugan, C.-C. Hu, Y.-F. Duann and R.-J. Chung, Poly(methyl methacrylate) in orthopedics: Strategies, challenges, and prospects in bone tissue engineering, *Polymers*, 2024, **16**(3), 367, DOI: 10.3390/polyml6030367.

75 H. H. Tuson, G. K. Auer, L. D. Renner, M. Hasebe, C. Tropini, M. Salick, W. C. Crone, A. Gopinathan, K. C. Huang and D. B. Weibel, Measuring the stiffness of bacterial cells from growth rates in hydrogels of tunable elasticity, *Mol. Microbiol.*, 2012, **84**(5), 874–891, DOI: 10.1111/j.l365-2958.2012.08063.x.

76 S. Syed, A. Karadaghy and S. Zustiak, Simple polyacrylamide-based multiwell stiffness assay for the study ofstiffness-dependent cell responses, *J. Visualized Exp.*, 2015, **97**, 52643, DOI: 10.3791/52643.

77 B. Le Roi and J. M. Grolman, Hydration effects driving network remodeling in hydrogels during cyclic loading, *ACS Macro Lett.*, 2025, **14**(2), 176–181, DOI: 10.1021/acsmacrolett.4c00653.

78 J. A. Kingston, N. J. Dunne, L. Looney and G. B. McGuinness, Effect of curing characteristics on residual stress generation in polymethyl methacrylate bone cements, *Proc. Inst. Mech. Eng., Part H*, 2008, **222**(6), 933–945, DOI: 10.1243/09544119JEIM343.

79 Q. Xin, Durability and reliability in diesel engine system design, in *Diesel Engine System Design*, Woodhead Publishing, 2013, pp. 113–202, ISBN 978-1-84569-715-0.

80 W. Ym, Z. Xie, Y. Ym, J. Yi, X. Liu, H. Wu, S. Wang, Y. Xie and Y. Yang, Aging behavior and lifetime prediction of PMMA under tensile stress and liquid scintillator conditions, *Adv. Ind. Eng. Polym. Res.*, 2019, **2**(2), 82–87, DOI: 10.1016/j.aiepr.2019.04.002.

81 V. Janas, F. Rodriguez and C. Cohen. Aging and thermodynamics of polyacrylamide gels. *Macromolecules*, 13(4):977–983, 1980, DOI: 10.1021/ma60076a042.AmericanChemicalSociety.

82 X. Zhang, Z. Lin, S. Xu, B. Li, Y. Guo, Y. Liu, S. Xiao, C. Zhang and G. Wu, Lifetime prediction and aging characteristics of silicone rubber under synergistic heat-moisture interaction, *Eng. Failure Anal.*, 2025, **170**, 109252, DOI: 10.1016/j.engfailanal.2024.109252.

83 V. S. Barbosa and C. Ruggieri, Fracture toughness testing using non-standard bend specimens part II: Experiments and evaluation of reference temperature for a low alloy structural steel, *Eng. Fract. Mech.*, 2018, **195**, 297–312, DOI: 10.1016/j.engfracmech.2018.03.028.

84 B. Sanborn, B. Song, A. Thompson, B. Reece and S. Attaway, High strain rate tensile response of a572 and 4140 steel, *Procedia Eng.*, 2017, **197**, 33–41, DOI: 10.1016/j.proeng.2017.08.079.

85 L. Grandy and J. Mauzeroll, Localising the electrochemistry of corrosion fatigue, *Curr. Opin. Colloid Interface Sci.*, 2022, **61**, 101628, DOI: 10.1016/j.cocis.2022.101628.

86 A. Turmbull, Modeling of the chemistry and electrochemistry in cracksa review, *Corrosion*, 2001, **57**(2), 175–189, DOI: 10.5006/1.3290342.

87 H. H. Tuson, L. D. Renner and D. B. Weibel, Polyacrylamide hydrogels as substrates for studying bacteria, *Chem. Commun.*, 2012, **48**(10), 1595–1597, DOI: 10.1039/C1CC14705F.

88 J. Schindelin, I. Arganda-Carreras, E. Frise, V. Kaynig, M. Longair, T. Pietzsch, S. Preibisch, C. Rueden, S. Saalfeld, B. Schmid, J.-Y. Tinevez, D. J. White, V. Hartenstein, K. Eliceiri, P. Tomancak and A. Cardona, Fiji: an open-source platform for biological-image analysis, *Nat. Methods*, 2012, **9**(7), 676–682.

89 E. van Wijngaarden, T. Chen, L. L. Brito, N. Bouklas, A. Giometto and M. N. Silberstein. Data archive bacterial crack detection, 2025.

90 T. A. Gaidenko, T.-J. Kim and C. W. Price, The PrpC serine-threonine phosphatase and PrkC kinase have opposing physiological roles in stationary-phase bacillus sub-tilis cells, *J. Bacteriol.*, 2002, **184**(22), 6109–6114, DOI: 10.1128/jb.l84.22.6109-6114.2002.

91 H.-R. Hong, C. R. Prince, D. D. Tetreault, L. Wu and H. A. Feaga, YfmR is a translation factor that prevents ribosome stalling and cell death in the absence of EF-p, *Proc. Natl. Acad. Sci. U. S. A.*, 2024, **121**(8), e2314437121, DOI: 10.1073/pnas.2314437121.